Anisotropic Rabi model with two-photon relaxation

Hui Li,[*] Jia-Kai Shi,[*] Li-Bao Fan, Zi-Min Li,[†] and Chuan-Cun Shu[‡]
Institute of Quantum Physics, Hunan Key Laboratory of Nanophotonics and Devices, and Hunan Key Laboratory of Super-Microstructure and Ultrafast Process, School of Physics, Central South University, Changsha 410083, China

(Received 23 April 2024; revised 11 July 2024; accepted 12 July 2024; published 5 August 2024)

The interplay of three light-matter interaction processes, i.e., rotating and counterrotating interactions and two-photon relaxation of the light field, is a topic of interest in quantum optics and quantum information processing. In this work we investigate theoretically the three light-matter interaction processes using the anisotropic Rabi model, which accounts for different strengths of rotating and counterrotating interactions and the unique occurrence of photon escape exclusively in pairs. By numerically solving the Lindblad master equation, we analyze the excitation-relaxation dynamics and derive a non-Hermitian effective Hamiltonian to gain further physical insights. To explore the individual effects of these interactions, we examine three analytically tractable limits of the effective Hamiltonian. Our analysis reveals that the three competitive light-matter interaction processes exhibit sensitivity to parity, leading to intriguing phenomena in both transient and steady states. Particularly interesting dynamical patterns resembling quantum phase transitions emerge when these three interaction terms compete. This work deepens the understanding of ultrastrong light-matter interaction in open quantum systems and offers valuable insights into cavity-based quantum computations.

DOI: 10.1103/PhysRevA.110.023708

I. INTRODUCTION

The quantum Rabi model (QRM), which characterizes the dynamic interplay between a two-level quantum system (referred to as a qubit) and a single-mode quantized light field confined within a cavity, stands as one of the most elementary interaction physical models [1–7]. Despite its fundamental nature, the QRM manifests a diverse array of physical phenomena and has discovered practical utility across an extensive spectrum of scientific disciplines. These include, but are not limited to, the realms of quantum optics [8], condensed-matter physics [9,10], and the forefront of cutting-edge quantum technologies [11,12].

The QRM features a competitive interplay between two distinct modes of light-matter interaction: the rotating terms (RTs) and the counterrotating terms (CRTs). The RTs characterize processes involving the exchange of excitations between the qubit and the cavity, preserving the total excitation count. In contrast, the CRTs give rise to events where both a qubit excitation and a photon are simultaneously created or annihilated, maintaining only the parity of the excitation number. The conservation of parity within the QRM leads to a multitude of significant physical consequences, including its solvability [2,6,13–15], the emergence of level crossing points [16,17], the presence of hidden symmetries [18–21], and the occurrence of a superradiant phase transition [22–25].

While most research on the QRM has focused on idealized closed systems without relaxation, real-world situations involve environmental influences. Accounting for the environment requires the use of the Lindblad master equation. In certain cases, a non-Hermitian effective Hamiltonian can be derived to describe the system in the Schrödinger formalism, offering deeper physical insights. For example, an intriguing two-photon relaxation process has been postulated and investigated [26–28]. In this context, the escape of photons from a cavity occurs exclusively in pairs, preserving the conservation of parity within the QRM. As a consequence, the excitation-relaxation dynamics of the system, including both transient and steady states, exhibits a sensitivity to parity, giving rise to various remarkable phenomena that are absent in the closed QRM. The two-photon relaxation mechanism has been proposed to facilitate universal quantum computing. Specifically, it has been theoretically and experimentally demonstrated that any initial state of the cavity, subjected to two-photon relaxation, evolves into two Schrödinger cat states, resulting in a qubit that relies on the characteristics of a cavity [28–34]. The intricate interplay between the light-matter interaction and the two-photon relaxation has been explored in Ref. [27]. However, there is still a lack of comprehensive understanding regarding the competitive dynamics involving RTs, CRTs, and relaxation terms.

In this work we adopt the theoretical framework established in Ref. [27] and investigate the competition among different interaction processes. Specifically, we consider the anisotropic Rabi model, which has been extensively studied in previous works [35–45]. In this model, the coupling strengths of the RTs and CRTs are different. By adjusting the coupling strengths and the two-photon relaxation rate, we find that the excitation-relaxation dynamics exhibits interesting parity-sensitive behavior in both transient and steady states. We explain these phenomena by analyzing the competition

[*]These authors contributed equally to this work.
[†]Contact author: zimin.li@csu.edu.cn
[‡]Contact author: cc.shu@csu.edu.cn

among different interaction processes. To achieve this, we numerically solve the quantum master equation and utilize the effective Hamiltonian to gain further physical insights.

The structure of this paper is as follows. In Sec. II we present the system Hamiltonian and the Lindblad master equation that incorporates two-photon relaxation. We subsequently explore three solvable limits in Sec. III, which are indicative of the effects arising from distinct transition processes. Section IV showcases exceptional phenomena observed in both transient dynamics and steady states. These are elucidated by examining the underlying principles of competitive interactions. A summary is given in Sec. V.

II. MODEL HAMILTONIAN

We employ the anisotropic Rabi model (ARM) [35,36,39,46] to examine the consequences of distinct light-matter interaction components. Different from dealing with the standard QRM, we encounter two types of interactions characterized by different strengths in the ARM. The ARM Hamiltonian reads

$$\mathcal{H} = \mathcal{H}_0 + \mathcal{H}_1 + \mathcal{H}_2, \tag{1}$$

where the free Hamiltonian $\mathcal{H}_0$, the Jaynes-Cummings interaction Hamiltonian $\mathcal{H}_1$, and the counterrotating interaction Hamiltonian $\mathcal{H}_2$ are given by ($\hbar = 1$)

$$\begin{aligned}\mathcal{H}_0 &= \omega a^\dagger a + \frac{\Delta}{2}\sigma_z,\\ \mathcal{H}_1 &= g_1(a\sigma_+ + a^\dagger\sigma_-),\\ \mathcal{H}_2 &= g_2(a^\dagger\sigma_+ + a\sigma_-).\end{aligned} \tag{2}$$

Here $a^\dagger$ and a are the creation and annihilation operators for the quantized light field in the cavity, with a resonance frequency ω. Meanwhile, $\sigma_z = |e\rangle\langle e| - |g\rangle\langle g|$, $\sigma_+ = |e\rangle\langle g|$, and $\sigma_- = |g\rangle\langle e|$ are the atomic raising and lowering operators linked to the qubit with a transition frequency Δ. The two types of interactions between the cavity and qubit are characterized by the coupling strengths g_1 and g_2. The ARM simplifies to the standard QRM with $g_1 = g_2$. When $g_2 = 0$, it transforms into the Jaynes-Cummings model (JCM). When $g_1 = 0$, it corresponds to the anti-JCM (AJCM). Physical implementations or simulations of the QRM and ARM are achievable, e.g., in circuit quantum electrodynamics setups [11,39] and in synthetic antiferromagnets with intrinsic asymmetry of magnetic anisotropy [47].

The Hamiltonian has Z_2 symmetry in the sense that it is invariant under the parity transformation generated by the combined parity operator

$$\mathcal{P} = -\sigma_z e^{i\pi a^\dagger a}. \tag{3}$$

As a physical consequence, the ARM conserves the parity of the total excitation number in the system [18]. To be specific, we consider the photon-qubit bare basis, defined by $|n, e(g)\rangle \equiv |n\rangle \otimes |e(g)\rangle$, with $|n\rangle$ the Fock states and $|e\rangle$ and $|g\rangle$ the excited and ground states of σ_z. Owing to the conserved parity, from an initial state with definite parity, the evolution under the ARM Hamiltonian goes along the corresponding parity chain [27,48], given by

$$\begin{aligned} p = +1, &\quad \{|0, g\rangle, |1, e\rangle, |2, g\rangle, |3, e\rangle, \dots\},\\ p = -1, &\quad \{|0, e\rangle, |1, g\rangle, |2, e\rangle, |3, g\rangle, \dots\}. \end{aligned} \tag{4}$$

Regarding the effects of the environment, a relaxation scheme where photons can only leak in pairs has been investigated [27]. In this case, the dissipation does not break the parity conservation, and the dynamical behaviors are expected to be parity sensitive, i.e., different for initial states from two parity subspaces.

When two-photon relaxation is considered, the time-dependent density matrix $\rho(t)$ of the system can be described by the Lindblad master equation [49–51]

$$\dot{\rho}(t) = -i[\mathcal{H}, \rho(t)] + 2\kappa a^2\rho(t)(a^\dagger)^2 - \kappa\{(a^\dagger)^2a^2, \rho(t)\}, \tag{5}$$

with κ the relaxation rate. By rearranging Eq. (5) we obtain

$$\dot{\rho}(t) = -i[\mathcal{H}_{\text{eff}}\rho(t) - \rho(t)\mathcal{H}_{\text{eff}}^\dagger] + \mathcal{L}_{\text{jump}}(\rho), \tag{6}$$

with the effective Hamiltonian

$$\mathcal{H}_{\text{eff}} = \mathcal{H} - i\kappa(a^\dagger)^2a^2 \tag{7}$$

and the quantum jump operator

$$\mathcal{L}_{\text{jump}}(\rho) = 2\kappa a^2\rho(t)(a^\dagger)^2. \tag{8}$$

When the quantum jump effects can be neglected, the dynamics of the system can be approximately described in the Schrödinger formalism with the effective Hamiltonian $\mathcal{H}_{\text{eff}}$. The imaginary parts of the eigenvalues of $\mathcal{H}_{\text{eff}}$ represent the decays of the eigenstates and thus the leaks of probabilities from the system into the environment. Therefore, when calculating the expectation value of a physical observable in non-Hermitian systems, one needs to renormalize the wave function. Specifically, the imaginary term $i\kappa(a^\dagger)^2a^2$ in Eq. (7) indicates that higher photon levels have larger decay rates and thus decrease faster in probabilities. As a result, the states with slower photon decay become dominant. This is effectively a relaxation process with probabilities transiting from high photon levels to low photon levels, coinciding with the effects of the quantum jump operator $\mathcal{L}_{\text{jump}}(\rho)$. In this way, the time-dependent Schrödinger equation of the effective Hamiltonian captures the main features of the dynamics apart from the quantum jump effects.

Figure 1 shows the transition diagram induced by the rotating interaction $\mathcal{H}_1$, the counterrotating term $\mathcal{H}_2$, and the quantum jump operator $\mathcal{L}_{\text{jump}}(\rho)$. The rotating interactions (denoted by green arrows between $|n, e\rangle$ and $|n+1, g\rangle$) exchange excitations between the qubit and the cavity and thus conserve the total number of excitations. The CRTs (indicated by blue arrows between $|n, g\rangle$ and $|n+1, e\rangle$) create (or annihilate) excitations in both the qubit and cavity simultaneously and thus only conserve the parity of excitation numbers. The quantum jump operator $\mathcal{L}_{\text{jump}}(\rho)$ (shown by red arrows) only happens from high levels to low levels. The decay rates are larger in the states with more photons. The interplay of these processes induces the exotic dynamical behaviors of the system.

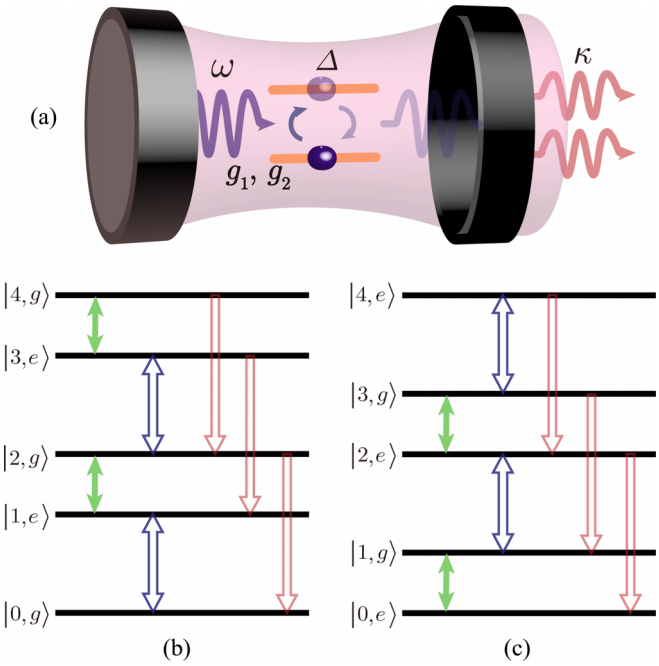

FIG. 1. (a) Schematic of the anisotropic Rabi model with two-photon relaxation. Also illustrated are the possible transitions induced by the rotating interaction terms (green), counterrotating terms (blue), and the two-photon relaxation term (red) in (b) even- and (c) odd-parity subspaces of the photon-qubit bare basis.

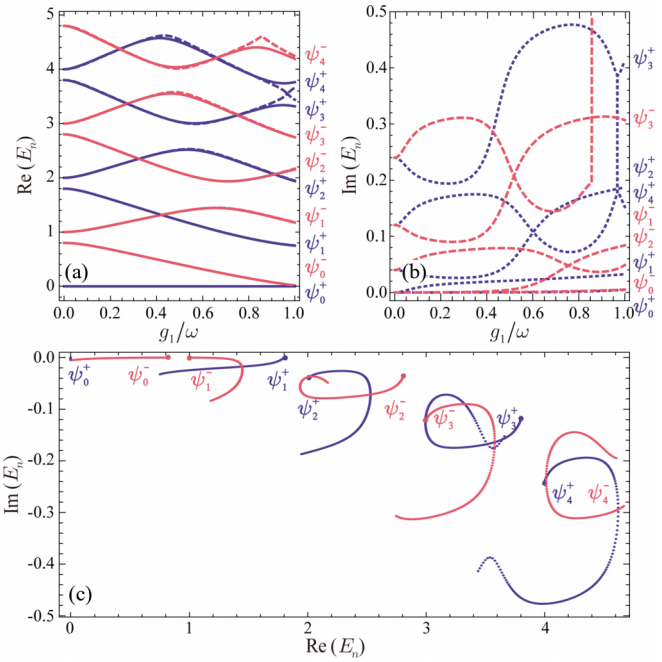

FIG. 2. (a) Real and (b) imaginary parts of the eigenvalues of the ARM with (dashed lines) or without (solid lines) two-photon relaxation, versus the coupling strength g_1/ω. (c) Eigenvalues of the system Hamiltonian on the complex plane with various values of the coupling strength g_1/ω. The fixed parameters are $\Delta/\omega = 0.8$, $\kappa/\omega = 0.02$, and $\lambda = g_2/g_1 = 0.5$.

III. COMPLEX ENERGY SPECTRUM

A. Spectrum of the effective Hamiltonian

As mentioned, the open-system dynamics can be described by the Schrödinger equation of the effective non-Hermitian Hamiltonian. In the following, we analyze the spectrum of this Hamiltonian.

There is no simple closed-form solution to the ARM and we thus rely on numerical diagonalization, as well as approximations. We first calculate the spectrum by numerical diagonalization and give physical interpretations of the complex eigenvalues. The spectrum is complex, as shown in Fig. 2. The real parts of eigenvalues denote the frequencies and the imaginary parts characterize the effective decay rates. In Fig. 2 the eigenvalues are labeled with ψ_n^p, where n is the level index and the value of p takes $+$ for even-parity subspace and $-$ for odd-parity subspace.

The non-Hermitian term $i\kappa(a^\dagger)^2a^2$ in the effective Hamiltonian does not directly induce any transition between bare states. However, it contributes imaginary eigenvalues associated with different photon numbers and thus effectively results in decay processes. Therefore, the effective decay term in the Schrödinger formalism approximates the effects of the relaxation processes in the Lindblad formalism. In this way, we see intuitively how the non-Hermitian effective Hamiltonian can describe the full dynamics that are determined by the quantum master equation.

We turn to solvable limits of the effective Hamiltonian for further physical intuition. The JCM and AJCM are both exactly solvable and thus the effects of the RTs and CRTs can be analyzed separately. From the analytic results, we can deduce the competition between different types of interactions. Even the trivial decoupled limit, with $g_1 = g_2 = 0$, provides additional intuition to the decay process.

B. Decoupled limit

With $g_1 = g_2 = 0$, the qubit is decoupled from the field and the effective Hamiltonian becomes

$$\mathcal{H}_{\rm eff}^{g=0} = \mathcal{H}_0 - i\kappa(a^\dagger)^2a^2. \tag{9}$$

This case is trivially solvable with the eigenvalues given as

$$E_{n,g=0}^{\pm} = n\omega \pm \frac{\Delta}{2} - i\kappa n(n-1) \tag{10}$$

and the eigenstates are simply bare states

$$\psi_{n,g=0}^{\pm} = |n,\pm\rangle \equiv |n\rangle \otimes |\pm\rangle\,. \tag{11}$$

We see from the eigenvalues that the decay rates of eigenstates increase with the photon number.

C. Jaynes-Cummings model

When g_2 is set to 0 and only rotating interactions are taken into account, we reach the JCM [52–55]. The effective Hamiltonian now reads

$$\mathcal{H}_{\rm eff}^{\rm JC} = \mathcal{H}_0 + g_1(a\sigma_+ + a^\dagger\sigma_-) - i\kappa(a^\dagger)^2a^2, \tag{12}$$

which is exactly solvable. The eigenvalues are

$$E_{n,\pm}^{\rm JC} = \left(n+\tfrac{1}{2}\right)\omega - i\kappa n^2 \pm \tfrac{1}{2}\sqrt{(A_n^-)^2 + B_n^2}, \tag{13}$$

where

$$A_n^{\pm} = (\omega \pm \Delta) - 2i\kappa n, \;\; B_n = 2g\sqrt{n+1}. \tag{14}$$

The definition of A_n^+ will be used for the anti-Jaynes-Cummings model later.

A special case that can be analytically dealt with is when the qubit and cavity are in resonance, with $\delta = \omega - \Delta = 0$. The corresponding eigenvalues are

$$E_{n,\pm}^{\mathrm{JC}} = \left(n + \tfrac{1}{2}\right)\omega - i\kappa n^2 \pm \sqrt{(n+1)g_1^2 - n^2\kappa^2}. \tag{15}$$

The two eigenstates with the same index n are degenerate when the square root in Eq. (15) is 0, leading to an exceptional point due to the passive parity-time ($\mathcal{PT}$) symmetry (see further discussion in Appendix D).

D. Anti-Jaynes-Cummings model

We now consider the anti-JCM to explore the effects brought by CRTs. The effective Hamiltonian now reads

$$\mathcal{H}_{\mathrm{eff}}^{\mathrm{AJC}} = \mathcal{H}_0 + g_2(a^\dagger\sigma_+ + a\sigma_-) - i\kappa(a^\dagger)^2a^2, \tag{16}$$

which is also exactly solvable. The corresponding eigenvalues are

$$E_{n,\pm}^{\mathrm{AJC}} = \left(n + \tfrac{1}{2}\right)\omega - i\kappa n^2 \pm \tfrac{1}{2}\sqrt{(A_n^+)^2 + B_n^2}, \tag{17}$$

with A_n^+ and B_n given in Eq. (14).

IV. EXCITATION AND RELAXATION DYNAMICS

In this section we analyze the dynamics of the ARM with two-photon relaxation. To this end, we tune the coupling strengths g_1 and g_2, as well as the two-photon relaxation rate κ, to explore the interplay and competition of the different interaction terms.

We focus on both transient states and steady states by calculating the corresponding physical observables, namely, the cavity photon number and the qubit population. In particular, we discuss the excitation-relaxation dynamics with three approaches. First, we calculate the dynamics by numerically solving the Lindblad master equation with a specific initial state $\rho(0)$. We illustrate the overall dynamics in two parity subspaces and discuss the transient and steady states in detail. Second, we map the bare states onto the eigenbasis of the effective Hamiltonian and understand the relaxation dynamics by interpreting the corresponding complex eigenvalues as decay rates. Third, we understand some interesting steady-state behaviors from the perspective of the transition processes of the bare states.

A. Dynamical effects of the interaction terms

To begin with, we intuitively analyze the impact of the three types of interactions on the system dynamics. The relaxation processes involved in Eq. (5) is the simplest case as it does not include the interaction with the qubit. In addition, there is no process to regenerate photons into the system after the dissipation. In the decoupled limit, if we start from a bare state $|n, e(g)\rangle$, photons will decay at an exponential rate given by $\kappa n(n-1)$ and the cavity reaches the vacuum state $|0, e(g)\rangle$ if n is even. For initial states with odd photons, however, there will be a single photon left in the system since there is no mechanism to dissipate it. Since the qubit and cavity are decoupled in this limit, the qubit state is immune to relaxation and remains unchanged.

As shown in Fig. 1, the Jaynes-Cummings (JC) interaction terms generate transitions within subspaces that conserve excitation numbers. This leads to Rabi oscillations between two basis states that share the same number of excitations. In particular, if we start with the initial state $|n, e\rangle$, the probability of state $|n+1, g\rangle$ is oscillatory, given by

$$P_{|n+1,g\rangle}^{\mathrm{JC}} = \frac{4g_1^2(n+1)}{\left(\Omega_n^{\mathrm{JC}}\right)^2}\sin^2\left(\frac{\Omega_n^{\mathrm{JC}}t}{2}\right), \tag{18}$$

with the Rabi frequencies

$$\Omega_n^{\mathrm{JC}} = \sqrt{(\omega-\Delta)^2 + 4g_1^2(n+1)}. \tag{19}$$

Equation (18) shows that the complete population transfer only occurs in the resonant case. The oscillation frequencies increase with the coupling strength g_1 and the photon number n.

Different from the JC interaction terms, the CRTs induce transitions where two excitations emerge or disappear simultaneously, leading to anti-Rabi oscillations. With the initial state being $|n, g\rangle$, the population of the state $|n+1, e\rangle$ is given by

$$P_{|n+1,e\rangle}^{\mathrm{AJC}} = \frac{4g_2^2(n+1)}{\left(\Omega_n^{\mathrm{AJC}}\right)^2}\sin^2\left(\frac{\Omega_n^{\mathrm{AJC}}t}{2}\right), \tag{20}$$

with the anti-Rabi frequencies

$$\Omega_n^{\mathrm{AJC}} = \sqrt{(\omega+\Delta)^2 + 4g_2^2(n+1)}. \tag{21}$$

We can observe from the above equations that for small values of g_2, the frequencies are large while the amplitudes are small. Therefore, the effects of CRTs are negligible for small g_2 but prominent for large g_2.

The intricate interplay of the above dynamical processes leads to the interesting time evolution of the full system.

B. Transient states

We now start our discussion on the dynamics with the transient states in the even-parity subspace. The full dynamics with even parity is presented in Fig. 3. The system is initially prepared in the bare state $|2, g\rangle$, indicating that there are two photons in the cavity and the qubit is in its ground state at $t = 0$. We calculate the mean photon number and qubit population by solving the Lindblad master equation numerically. In the calculations, we set $g_2/g_1 = \lambda$ and vary the value of g_1 to obtain the dynamics concerning coupling strengths. To better see how RTs and CRTs interact with the relaxation separately, we choose the coupling ratio $\lambda = 0.5$ to further suppress the effects of CRTs for lower coupling strength regimes. The overall results are displayed in Figs. 3(a) and 3(b). It is clear that the interplay of the three types of interactions depends on the coupling strengths. The dynamical behaviors can be physically interpreted from the perspective of transition processes induced by the three types of interactions, as illustrated in Fig. 1(a).

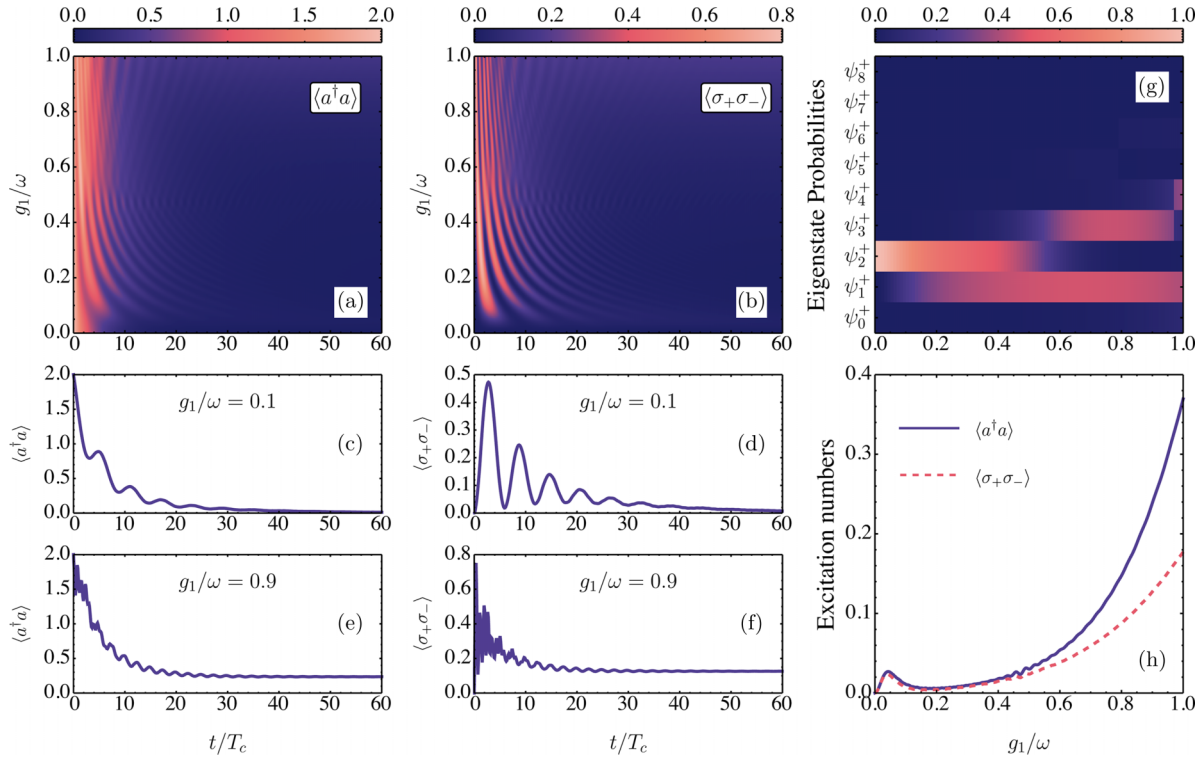

FIG. 3. Excitation-relaxation dynamics of the ARM in even-parity subspace, with the initial state $|2, g\rangle$ and parameters $\lambda = g_2/g_1 = 0.5$, $\Delta/\omega = 0.8$, and $\kappa/\omega = 0.02$. Shown is the time evolution of (a), (c), and (e) the mean photon number and (b), (d), and (f) the qubit population with various values of coupling strength g_1/ω in the time range of t/T_c, with $T_c \equiv \pi/\omega$. (g) Probability of eigenstates when mapping the initial state onto the eigenbasis. (h) Transient states of the mean photon number and qubit population with various values of coupling strength g_1/ω at time $t/T_c = 60$.

We take the case $g_1/\omega = 0.1$ as the first example, with the corresponding cavity photon number and qubit population displayed in Figs. 3(c) and 3(d), respectively. The ripples for short-range time mainly result from the interplay between the JC interactions and the two-photon relaxation, since the effects of CRTs are weak with the marginal value of $g_2/\omega = 0.05$. Through the relaxation channel $|2, g\rangle \Rightarrow |0, g\rangle$, the two photons in the initial state quickly escape from the cavity with a certain probability. Meanwhile, the Rabi oscillations transfer some of the population through the process $|2, g\rangle \leftrightarrow |1, e\rangle$ and thus prevent the relaxation. The effect of Rabi oscillations can be more obviously observed from the qubit dynamics in Fig. 3(d), where the qubit is not directly affected by the relaxation process and undergoes several periods of oscillations at the constant Rabi frequency. Later on, since the Rabi oscillations are reversible, the reexcited population undergoes relaxation again, which gives rise to an overall decaying behavior for both the cavity and qubit. Consequently, after several periods of Rabi oscillations, the population concentrates in the state $|0, g\rangle$, with both the cavity and qubit sitting around their ground states.

When g_1 increases, the effects of CRTs become nonnegligible, and the interference between these effects leads to nontrivial dynamical patterns. To demonstrate this, we take the case $g_1/\omega = 0.9$, and thus $g_2/\omega = 0.45$, as an example. The results are displayed in Figs. 3(e) and 3(f). The current case has two main differences from the previous one: The photons decay slower at the initial stage and more photons are left in the cavity in the final state. Since CRTs induce fast small-amplitude oscillations, the dynamics at beginning times are largely different from the previous case. For this time range, the main transition channel due to the competition between CRTs and relaxation is

$$|2, g\rangle \Leftrightarrow |3, e\rangle \Rightarrow |1, e\rangle\,, \tag{22}$$

where the relaxation is weakened to a much greater extent. As a consequence, the mean photon number and qubit population in this case are both more than in the previous case at the beginning. After this initial competition, the reversible nature of Rabi and anti-Rabi oscillations still offers chances to the relaxation channel and thus leads to the overall decaying behavior. The relaxation processes smooth these oscillatory dynamics for a long time range, where all the transitions reach a dynamical equilibrium, with a higher number of excitations in the final state.

We note that any other initial states with even parity give rise to almost the same physics since they decay quickly to the bare state $|2, g\rangle$ that we consider in the above example. However, higher initial states will lead to more complicated dynamics at the beginning times, since the Rabi and anti-Rabi frequencies increase with photon number n. The final dynamical equilibrium only depends on the system parameters and the parity of the initial state, ignoring the specific form of the wave functions.

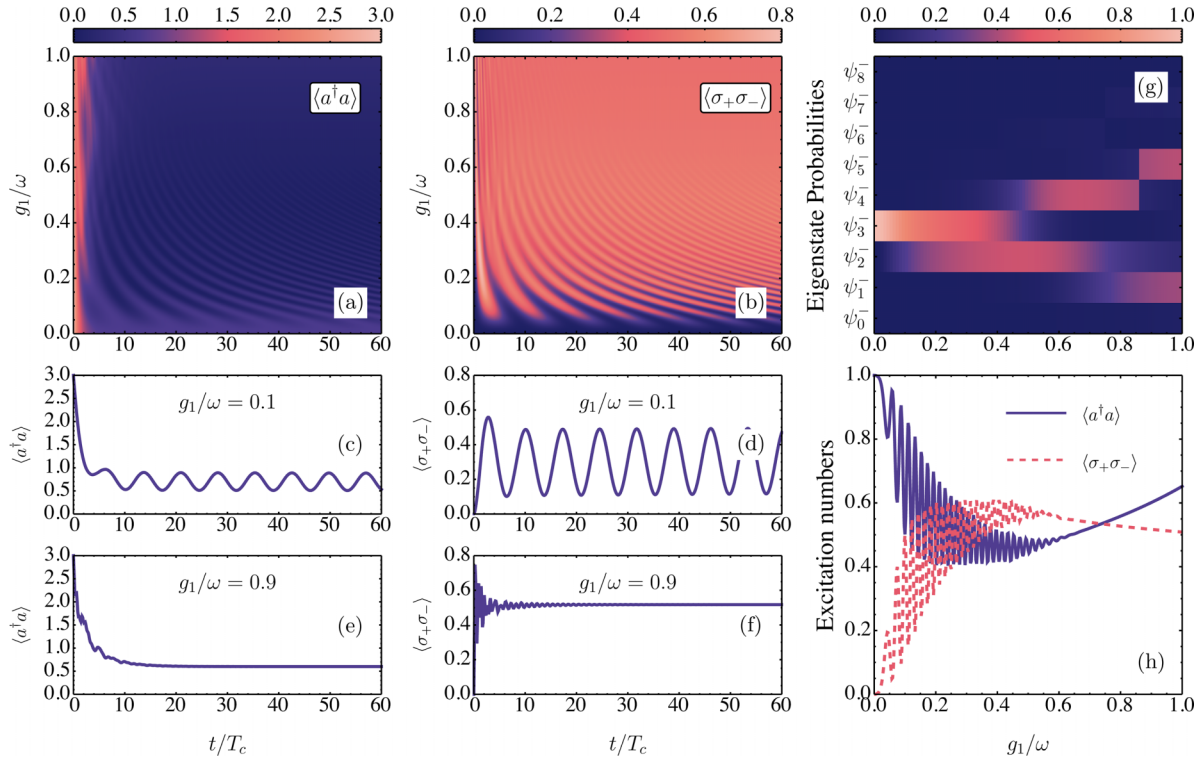

FIG. 4. Excitation-relaxation dynamics of the ARM in odd-parity subspace, with the initial state $|3, g\rangle$ and parameters $\lambda = g_2/g_1 = 0.5$, $\Delta/\omega = 0.8$, and $\kappa/\omega = 0.02$. Shown is the time evolution of (a), (c), and (e) the mean photon number and (b), (d), and (f) the qubit population with various values of coupling strength g_1/ω in the time range of t/T_c, with $T_c \equiv \pi/\omega$. (g) Probability of eigenstates when mapping the initial state onto the eigenbasis. (h) Transient states of the mean photon number and qubit population with various values of coupling strength g_1/ω at time $t/T_c = 60$.

If we focus on the medium-range time that is long (e.g., $t = 60\pi$ in our case), but not long enough for the system to reach the final steady state, we can see how the equilibrium is affected by the coupling strengths. For the even-parity subspace, we observe some dynamical behaviors that are rather steady, as illustrated in Fig. 3(d). These medium-range states are already quite similar to the final steady states except for the local maximum at around $g_1 = 0.05$. This peak was noticed in Ref. [27] and was believed to exist in the steady state for the coupling strength $g_1 = g_2 = \kappa$.

Here we show that this local maximum is absent in the final steady states and its position is irrelevant to the relaxation rate κ. It turns out to be a consequence of the competition between JC interactions and two-photon relaxation, which is most clearly seen in the dissipative JCM, where CRTs are absent. In a more direct interpretation, the local maximum originates from the slow Rabi oscillations for small g_1, whose position can be analytically determined from the JCM. We see from Eq. (19) that the Rabi frequency increases with the coupling strength g_1. Therefore, for a given time t, oscillations associated with different coupling strengths are going through various stages. There might be one that happens to be at its maximum, whereas the neighboring ones are not. At this specific time, we then observe the local maximum with respect to the coupling strength, as displayed in Fig. 3(h). With this reasoning, it is clear that the corresponding g_1 value decreases with time t and thus the peak disappears for a long enough time.

Since the total system conserves the parity of the total excitation number, the dynamics are expected to be parity sensitive. Indeed, the results with the initial odd-parity state $|3, g\rangle$, shown in Fig. 4, demonstrate that the dynamics of both the cavity photon number and qubit population are significantly different from the even-parity case. The major difference is that the oscillations are much more persistent in odd subspace. The dynamics can also be understood in the same intuitive way and can be largely deduced from the solvable limits. In the decoupled case where $g_1 = g_2 = 0$, the initial state $|3, g\rangle$ quickly loses two photons and reaches the final state $|1, g\rangle$. In this case, no mechanism exists to excite the qubit or dissipate the photon. Things become more interesting when light-matter interactions are introduced. For small coupling strength, the system oscillates between states $|1, g\rangle$ and $|0, e\rangle$ owing to the JC interactions. If $g_2 = 0$, this oscillation persists forever and the steady state is never reached. This is verified by the constant oscillations depicted in Figs. 4(c) and 4(d). For nonzero g_2, however, the weak effects of CRTs induce a tiny number of transitions to higher photon states, which are then dissipated by the relaxation processes. This is the reason why the system can still reach steady state after long-time oscillations. When g_2 grows to the regimes where the effects of CRTs are prominent, the Rabi oscillations are destroyed by the CRTs and then quickly smoothed by the relaxation terms, as shown in Figs. 4(e) and 4(f). It is clear from the quasisteady states in Fig. 4(h) that the photon and qubit excitations left in the system are more than those of the even-parity case. This

is because there is always some population of $|1, g\rangle$ and $|0, e\rangle$ that cannot be dissipated.

Since the connections between the Lindblad master equation and the non-Hermitian effective Hamiltonians have been established in the previous sections, the overall dynamics can also be approximately understood with physical intuitions by mapping the initial state on the eigenbasis of the Hamiltonian (1). This mapping shows which modes are more active at a given value of g in each parity subspace. By doing so, we can check the corresponding frequencies and decay rates from Fig. 2 and thus understand the dynamical behavior. Here we map the initial bare state $|2, g\rangle$ onto the eigenstates of the effective Hamiltonian, and the probabilities of the eigenstates are displayed in Fig. 3(g). We observe that the dynamics exhibit decaying oscillations with rather steady frequencies for small g/ω, as shown in Figs. 3(c), 3(d), 4(c), and 4(d). Various eigenstates with different decay rates become non-negligible with increasing g/ω and thus lead to more complex dynamical patterns, as exemplified in Figs. 3(e), 3(f), 4(e), and 4(f). This phenomenon can be understood as an extension of the difference between the strong- and the ultrastrong-coupling regimes in the open system.

C. Steady states

After a long enough time, the system arrives at a dynamical equilibrium of the three types of transitions, i.e., the steady state. With steady states, it is easy to identify the interplay of the interaction processes. The steady states for the cavity and the qubit in even- and odd-parity subspaces are calculated with respect to the coupling strengths g_1 and g_2 and displayed in Figs. 5 and 6, respectively. We can observe different behaviors by following different paths on the $g_1 - g_2$ plane. For example, following the path $g_2 = 0$, we observe the steady states of the JCM with respect to g_1. On the other hand, we have the steady states of the AJCM with the constraint $g_1 = 0$. Setting $g_1 = g_2$, we have the standard QRM, which exhibits parabolic behaviors with respect to the coupling strengths. We note that the steady states are determined solely by the parity, rather than any specific forms, of the initial states. Nevertheless, for the sake of clarity and simplicity, we base our discussion on the particular initial states $|2, g\rangle$ for even parity and $|3, g\rangle$ for odd parity in the following.

To gain more physical intuition, we again turn to the three solvable limits and study the interplay of coupling and relaxation terms. For the even-parity case, the decoupled limit leads to the trivial consequence that both photons escape from the system through the relaxation $|2, g\rangle \Rightarrow |0, g\rangle$. Therefore, there is no photon in the cavity after a long enough time and the qubit stays in the ground state. In the JCM limit where $g_2 = 0$, the different situation gives rise to the same result. As can be seen from the transient states of the JCM, the Rabi oscillation for $|2, g\rangle \leftrightarrow |1, e\rangle$ diminishes with time because the total population decays exponentially to the vacuum bare state through the irreversible relaxation process $|2, g\rangle \Rightarrow |0, g\rangle$. With this, it is again verified that the small peak in Fig. 3(h) is not a steady state, but rather a quasisteady one.

Following another path $g_1 = 0$, the dynamics can be described by the AJCM, in which case the transition processes

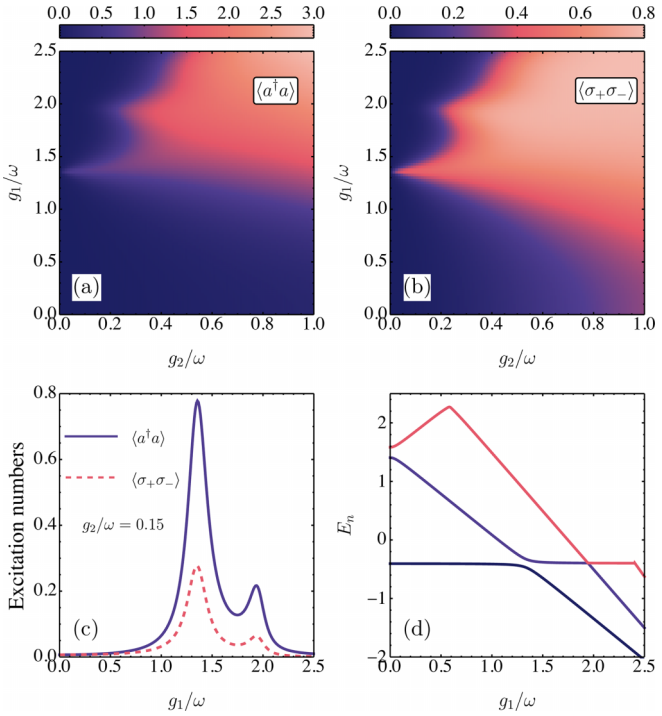

FIG. 5. (a) Cavity photon number and (b) qubit population in the steady state of even-parity subspace with respect to the coupling strengths g_1 and g_2. (c) Cavity photon number and qubit population with fixed coupling $g_2/\omega = 0.15$ and varying coupling strength g_1/ω. (d) Eigenvalue spectrum with the same parameter values as in (c). The peaks in (c) coincide with the avoided crossings in (d).

are more complicated. The anti-Rabi oscillation $|2, g\rangle \Leftrightarrow |3, e\rangle$ competes with the relaxation, leading to the lower-level anti-Rabi oscillation $|0, g\rangle \Leftrightarrow |1, e\rangle$ that is immune to the further relaxation process. The amount of population that is transferred by the anti-Rabi oscillation is determined by P_1^{AJC} in Eq. (20). Consequently, the excitation numbers in the AJCM case increase with the value of g_2. This anti-Rabi oscillation persists forever unless JC interactions associated with g_1 are introduced.

For the general case, with all three types of interactions present, the steady state of the ARM is a nontrivial mix of the JCM and AJCM with two-photon relaxation. Generally, the steady states of the cavity and qubit increase with respect to both g_1 and g_2, as can be observed from Figs. 5(a) and 5(b) for the cavity and qubit, respectively. The results along the path $g_1 = g_2$ are consistent with the results presented in Ref. [27]. A particularly interesting phenomenon, absent in the standard QRM, of the steady states in even-parity subspace is the peaks along g_1 with a small value of g_2, as shown in Fig. 5(c). These peaks are found sitting at the avoided level crossings of the eigenspectrum, as displayed in Fig. 5(d). These avoided crossings can be analytically determined by calculating genuine level crossings of the JCM. The position for the mth peak, with respect to g_1, is then given by

$$\frac{g_1}{\omega} = \sqrt{(2m-1) + \frac{\Delta}{\omega}}, \quad m \in \mathbb{N}_+. \tag{23}$$

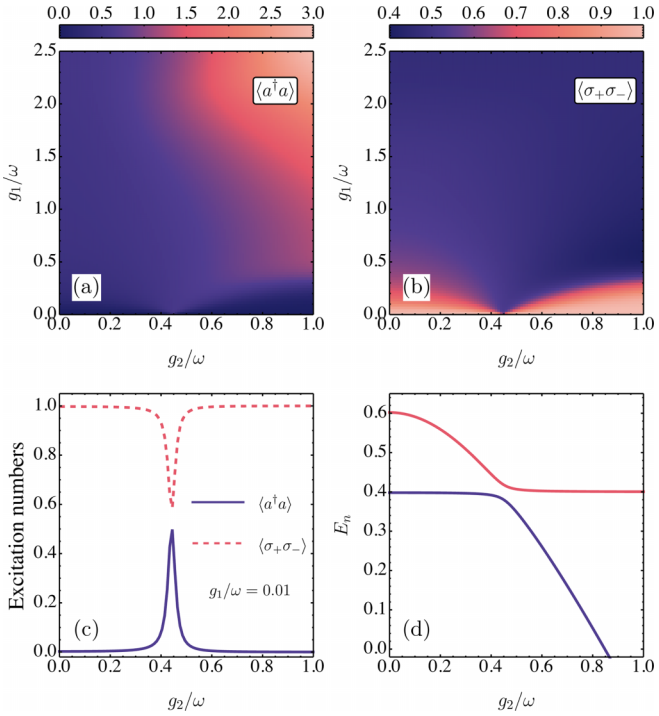

FIG. 6. (a) Cavity photon number and (b) qubit population in the steady state of odd-parity subspace with respect to the coupling strengths g_1 and g_2. (c) Cavity photon number and qubit population with fixed coupling $g_1/\omega = 0.01$ and varying coupling strength g_2/ω. (d) Eigenvalue spectrum with the same parameter values as in (c). The peak and valley in (c) coincide with the avoided crossing in (d).

To understand the physical origins of these peaks, we go back to the Hermitian case. We start with the JCM with U(1) symmetry. The energy levels in even-parity subspace cross with each other, since they now all belong to different symmetric sectors. If we add perturbative g_2 into the system, the U(1) symmetry is broken and reduced to the $\mathbb{Z}_2$ symmetry. Spectra with a specific parity subspace will repulse with each other, and thus the previous level crossings become avoided. At avoided crossings induced by small g_2, eigenstates strongly mix and thus the corresponding physical observables drastically change. In the JCM, the initial state $|0, g\rangle$ is the ground state in a one-dimensional subspace and it does not interact with any other eigenstates. When we switch on the CRTs with small g_2, the initial state $|0, g\rangle$ strongly interacts with other states at the avoided crossings. Since the initial state $|0, g\rangle$ is no longer the eigenstate of the system, the dynamics exhibits Rabi oscillation between the two original eigenstates at the avoided crossings. In the vicinity of the first peak at $g_1/\omega = \sqrt{1 + \Delta/\omega}$, the following oscillation occurs:

$$|0, g\rangle \leftrightarrow |1, -\rangle_{\rm JC}\,. \tag{24}$$

The JC eigenstate (or dressed state) $|1, -\rangle_{\rm JC}$, explicitly given in Eq. (C3), is a superposition of the bare states $|0, e\rangle$ and $|1, g\rangle$ and contains one excitation. Correspondingly, the photon number and qubit population oscillate between 0 and 1. With the relaxation process considered, the oscillations will be smoothed and arrive at steady states with larger mean photon numbers. In the meantime, for other values of g_1 that are far from the avoided crossings, the oscillation in Eq. (24) is weak and the final excitation is marginal. If the initial state is not $|0, g\rangle$, the JC interaction and relaxation will make the system jump to the lowest levels and thus lead to the same results as the initial $|0, g\rangle$.

As expected, the steady states in the odd-parity subspace are different in shape, as shown in Fig. 6. In the trivial decoupled limit, the initial state $|3, g\rangle$ irreversibly decays to the final state $|1, g\rangle$. In the JCM limit, the Rabi oscillation $|1, g\rangle \leftrightarrow |0, e\rangle$ persists forever, giving rise to the total excitation being 1. In the AJCM case, the reversible oscillation $|1, g\rangle \Leftrightarrow |2, e\rangle$ competes with the irreversible relaxation process $|2, e\rangle \Rightarrow |0, e\rangle$ and eventually transfers all population to the state $|0, e\rangle$. Similar to the even-parity case, we also observe a peak (valley) in the mean photon number displayed in Fig. 6(a) [the qubit population in Fig. 6(b)] at around $g_2/\omega = 0.42$, with very small g_1/ω. These local extrema result from the Rabi-type oscillation induced by avoided crossings, i.e.,

$$|0, g\rangle \leftrightarrow |0, -\rangle_{\rm AJC}\,, \tag{25}$$

where $|0, -\rangle_{\rm AJC}$ is a superposition of the bare states $|0, g\rangle$ and $|1, e\rangle$, as given in Eq. (C13). With simple calculations, we know that the avoided crossings are present at

$$\frac{g_2}{\omega} = \sqrt{(2m-1) - \frac{\Delta}{\omega}}, \quad m \in \mathbb{N}_+, \tag{26}$$

with a small value of g_1.

V. CONCLUSION

We have presented a detailed theoretical exploration of the interplay among three types of interactions, i.e., the Jaynes-Cummings interaction, the counterrotating terms, and the two-photon relaxation, within the framework of the anisotropic Rabi model. To comprehensively understand these competitive dynamics, we employed three approaches: numerical solution of the master equation, interpretation of the transition diagram induced by the interaction terms, and understanding of the dynamics through the eigenbasis of the effective Hamiltonian.

Our work provides insights into the dynamics of the cavity photon number and qubit population, elucidating their sensitivity to parity through analyzing three solvable limits of the non-Hermitian effective Hamiltonian. Specifically, we identified that the intriguing local maximum observed in the transient state for small g_1 is absent in the steady state, and our work provides an intuitive explanation for its origin. Furthermore, our work discovered peaks in the steady states of the cavity photon number and qubit population, which we attribute to avoided level crossings in the eigenvalue spectrum.

Our work contributes to a deeper understanding of the competition between Jaynes-Cummings interactions and counterrotating terms, as well as the effects of ultrastrong coupling in open quantum systems. We have clarified the effects of the quantum jump operator and offered a generalized framework for exploring the interplay among different

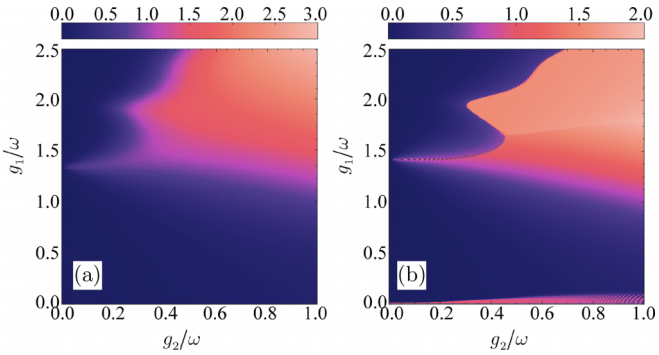

FIG. 7. Cavity photon number of the steady state in even-parity subspace, calculated through (a) the Lindblad master equation and (b) the TDSE of the non-Hermitian effective Hamiltonian, with $\Delta/\omega = 0.8$ and $\kappa/\omega = 0.02$.

types of interactions. These findings may have implications for cavity-based quantum computations.

ACKNOWLEDGMENTS

This work was supported by the National Natural Science Foundation of China Grants No. 12205383, No. 12274470, and No. 62273361;Hunan Provincial Natural Science Foundation of China Grant No. 2024JJ6483; and the Natural Science Foundation of Changsha Grant No. kq2202082.

APPENDIX A: DYNAMICS CALCULATED FROM THE NON-HERMITIAN EFFECTIVE HAMILTONIAN

We calculate the system dynamics by numerically solving the master equation in the main text. Here we study the changes in the cavity photon number and qubit population of the system with the coupling strength after an extended period of evolution, utilizing the time-dependent Schrödinger equation (TDSE) derived from the effective Hamiltonian. In addition, by comparing the results obtained by the two approaches, we find the crucial role of the quantum jump term in reaching the ultimate steady state.

The general states of the system can be extended in the order of the basis vectors of the Hilbert space. In the even-parity subspace, when the total photon number N is even, the system's state can be represented as

$$|\psi(t)\rangle = \sum_{n=0}^{N/2} C_{2n}^{g}(t)\,|2n, g\rangle + \sum_{n=0}^{N/2-1} C_{2n+1}^{e}(t)\,|2n+1, e\rangle\,, \tag{A1}$$

with the probability amplitudes $C_{2n}^{g}(t)$ and $C_{2n+1}^{e}(t)$, which can be obtained by solving the TDSE

$$i|\dot{\psi}(t)\rangle = H_{\text{eff}}\,|\psi(t)\rangle\,, \tag{A2}$$

with the initial state $|\psi(0)\rangle = |2, g\rangle$. As shown in Fig. 7, after a sufficiently long evolution time $10^3\pi$, we observe variations in $\langle a^\dagger a\rangle$ for different coupling strengths g_1 and g_2 under the evolution dominated by the effective Hamiltonian. The positions of characteristic peaks align with those obtained by solving the master equation. However, some oscillations are present in these steady state results, indicating they are not fully stabilized but rather more stable states.

The master-equation approach represents the behavior of the true final steady state due to its consideration of all effects including the quantum jump term $2\kappa a^2\rho(a^\dagger)^2$, whereas the effective Hamiltonian omits it. Therefore, we can conclude that the inclusion of the quantum jump terms allows the system to reach the ultimate steady state.

APPENDIX B: PHYSICAL INTERPRETATION OF THE LINDBLAD TERMS

In this Appendix we discuss the three dissipation terms in the Lindblad master equation. Here we consider two bare states in the basis of the main body system, defined as $|1\rangle = |n-2, g\rangle$ and $|2\rangle = |n, g\rangle$, which are connected by the two-photon relaxation. Consequently, the density operator can be expressed as $\rho = \sum_{i,j=1,2}\rho_{ij}\,|i\rangle\,\langle j|$ or in matrix form

$$\rho = \begin{pmatrix} \rho_{22} & \rho_{21} \\ \rho_{12} & \rho_{11} \end{pmatrix}, \tag{B1}$$

where the diagonal elements represent population ($\sum_i \rho_{ii} = 1$ with $\rho_{ii} \in \mathcal{R}_0^+$), while the off-diagonal elements denote coherence ($\rho_{ij} = \rho_{ji}^*$ with $\rho_{ij} \in \mathcal{C}$).

The dynamics of the system can be fully described by employing the Lindblad master equation, where the relaxation of photon pairs is represented by the dissipator

$$\mathcal{D}[a^2]\rho = 2\kappa a^2\rho(a^\dagger)^2 - \kappa(a^\dagger)^2a^2\rho - \kappa\rho(a^\dagger)^2a^2, \tag{B2}$$

with relaxation rate κ. The effect of the dissipator on the density operator can be divided into two parts: the continuous nonunitary dissipation terms given by $\kappa\{(a^\dagger)^2a^2, \rho\}$ and the quantum jump terms represented by $2\kappa a^2\rho(a^\dagger)^2$. We can obtain a matrix form for the dissipator as

$$\mathcal{D}[a^2]\rho = n(n-1)\begin{pmatrix} -2\kappa\rho_{22} & -\kappa\rho_{21} \\ -\kappa\rho_{12} & 2\kappa\rho_{22} \end{pmatrix}. \tag{B3}$$

By examining each term individually within this matrix, we intuitively reveal the effects of each element, specifically, (i) the nonunitary dissipation terms impact elements such as ρ_{21} and ρ_{12} along with coherence loss between bare states, which are represented by $-\kappa\rho_{21}$ and $-\kappa\rho_{12}$, respectively; (ii) the nonunitary dissipation terms also lead to energy and information losses from the upper state into the environment, related to $-2\kappa\rho_{22}$; and (iii) contrary to the effects mentioned above, the quantum jump terms contribute towards an increase in lower states' population, that is, $2\kappa\rho_{22}$. Overall, the excited number of the two bare states is conserved over time i.e., $\text{Tr}([\mathcal{D}[a^2]\rho) = 0$.

APPENDIX C: DERIVATIONS OF THE JC AND AJC RESULTS

In this Appendix we study the eigensystems of the JCM and AJCM with two-photon relaxation, whose Hilbert space splits into two unconnected parity chains due to the Z_2 symmetry.

When $g_2 = 0$, the adjacent states in each parity subspace are solely coupled by rotating terms, resulting in

Hilbert space partitioned into a collection of JC doublets $\{|n, e\rangle, |n+1, g\rangle\}$. The effective Hamiltonian of the JCM with two-photon relaxation can be expressed in matrix form as

$$H_{\text{eff}}^{\text{JC}} = \begin{pmatrix} \left(n+\frac{1}{2}\right)\omega - \frac{\delta}{2} - i\kappa n(n-1) & g_1\sqrt{n+1} \\ g_1\sqrt{n+1} & \left(n+\frac{1}{2}\right)\omega + \frac{\delta}{2} - i\kappa n(n+1) \end{pmatrix}, \tag{C1}$$

with $\delta = \omega - \Delta$ the detuning. The complex eigenvalues of the block Hamiltonian are given by

$$E_{n,\pm}^{\text{JC}} = \left(n+\tfrac{1}{2}\right)\omega - i\kappa n^2 \pm \tfrac{1}{2}\Omega_n^{\text{JC}}, \tag{C2}$$

with Rabi frequency $\Omega_n^{\text{JC}} = \sqrt{(\delta - 2i\kappa n)^2 + 4g_1^2(n+1)}$. Meanwhile, the corresponding eigenstates are found as

$$|n, +\rangle_{\text{JC}} = \cos\theta_n |n, e\rangle + \sin\theta_n |n+1, g\rangle, \tag{C3}$$

$$|n, -\rangle_{\text{JC}} = -\sin\theta_n |n, e\rangle + \cos\theta_n |n+1, g\rangle, \tag{C4}$$

where the probability coefficients in the states are defined as

$$\cos\theta_n = \sqrt{\frac{\Omega_n^{\text{JC}} - \delta + 2i\kappa n}{2\Omega_n^{\text{JC}}}}, \tag{C5}$$

$$\sin\theta_n = \sqrt{\frac{\Omega_n^{\text{JC}} + \delta - 2i\kappa n}{2\Omega_n^{\text{JC}}}}. \tag{C6}$$

Because of the excitation number conserving with this system, this leads to the Rabi oscillations between two bare states $|n, e\rangle$ and $|n+1, g\rangle$. In this way, we can assume the form of the time evolution of the system states as

$$|\psi(t)\rangle = \left[C_n^e(t)\,|n, e\rangle + C_{n+1}^g(t)\,|n+1, g\rangle\right] e^{-i(n+1/2)\omega t}, \tag{C7}$$

where $C_n^e(t)$ and $C_{n+1}^g(t)$ are time-dependent probability amplitudes for each state. Applying the TDSE $i|\dot{\psi}(t)\rangle = H_{\text{eff}}^{\text{JC}}|\psi(t)\rangle$, we then obtain the equations that the amplitudes satisfied,

$$\dot{C}_n^e(t) = \left(i\frac{\delta}{2} - \kappa n(n-1)\right) C_n^e(t) - ig_1\sqrt{n+1}\,C_{n+1}^g(t),$$

$$\dot{C}_{n+1}^g(t) = \left(-i\frac{\delta}{2} - \kappa n(n+1)\right) C_{n+1}^g(t) - ig_1\sqrt{n+1}\,C_n^e(t). \tag{C8}$$

When the initial states meet $C_n^e(0) = 1$, $C_{n+1}^g(0) = 0$, and $\delta = 0$, we can calculate the time evolution equation of the system state as

$$|\psi(t)\rangle = \left[\left(\cos\frac{\Omega_n^{\text{JC}}t}{2} + \frac{2\kappa n}{\Omega_n^{\text{JC}}}\sin\frac{\Omega_n^{\text{JC}}t}{2}\right)|n, e\rangle - i\frac{2g_1\sqrt{n+1}}{\Omega_n^{\text{JC}}} \times \sin\frac{\Omega_n^{\text{JC}}t}{2}\,|n+1, g\rangle\right] e^{-i(n+1/2)\omega t - \kappa n^2 t}. \tag{C9}$$

We then obtain the time-dependent population on state $|n+1, g\rangle$,

$$P_{|n+1,g\rangle}^{\text{JC}} = \frac{4g_1^2(n+1)}{\left(\Omega_n^{\text{JC}}\right)^2}\sin^2\left(\frac{\Omega_n^{\text{JC}}t}{2}\right). \tag{C10}$$

Similarly, when $g_1 = 0$, the ARM is reduced to the AJCM where adjacent states within each parity subspace are solely coupled through counterrotating terms, and thus the Hilbert space is divided into blocks spanned by the basis $\{|n+1, e\rangle, |n, g\rangle\}$. Consequently, the effective Hamiltonian of the AJCM with two-photon relaxation can be written in matrix form as

$$H_{\text{eff}}^{\text{AJCM}} = \begin{pmatrix} \left(n+\frac{1}{2}\right)\omega + \frac{\xi}{2} - i\kappa n(n+1) & g_2\sqrt{n+1} \\ g_2\sqrt{n+1} & \left(n+\frac{1}{2}\right)\omega - \frac{\xi}{2} - i\kappa n(n-1) \end{pmatrix}, \tag{C11}$$

with $\xi = \omega + \Delta$. Then the complex eigenvalues of the partitioned matrix are given by

$$E_{n,\pm}^{\text{AJC}} = \left(n+\tfrac{1}{2}\right)\omega - i\kappa n^2 \pm \tfrac{1}{2}\Omega_n^{\text{AJC}}, \tag{C12}$$

with $\Omega_n^{\text{AJC}} = \sqrt{(\xi - 2i\kappa n)^2 + 4g_2^2(n+1)}$ the Rabi frequency. The eigenstates can also be obtained as

$$|n, +\rangle_{\text{AJC}} = \cos\varphi_n |n+1, e\rangle + \sin\varphi_n |n, g\rangle, \tag{C13}$$

$$|n, -\rangle_{\text{AJC}} = -\sin\varphi_n |n+1, e\rangle + \cos\varphi_n |n, g\rangle, \tag{C14}$$

with

$$\cos\varphi_n = \sqrt{\frac{\Omega_n^{\text{AJC}} + \xi - 2i\kappa n}{2\Omega_n^{\text{AJC}}}}, \tag{C15}$$

$$\sin\varphi_n = \sqrt{\frac{\Omega_n^{\text{AJC}} - \xi + 2i\kappa n}{2\Omega_n^{\text{AJC}}}}. \tag{C16}$$

Because of the counterrotating terms, when the initial state of the system is $|n+1, e\rangle$, only $|g, n\rangle$ state can be coupled with it. Then we can assume the form of the time evolution of the system states as

$$|\phi(t)\rangle = \left[C_{n+1}^e(t)\,|n+1, e\rangle + C_n^g(t)\,|g, n\rangle\right] e^{-i(n+1/2)\omega t}, \tag{C17}$$

with $C_{n+1}^e(t)$ and $C_n^g(t)$ denoting the time-dependent probability amplitudes for each state. Using the TDSE $i|\dot{\phi}(t)\rangle = H_{\text{eff}}^{\text{AJC}}|\phi(t)\rangle$, we then get the equations that the amplitudes

satisfied,

$$\dot{C}^e_{n+1}(t) = \left(-i\frac{\xi}{2} - \kappa n(n+1)\right)C^e_{n+1}(t) - ig_2\sqrt{n+1}C^g_n(t),$$
$$\dot{C}^g_n(t) = \left(i\frac{\xi}{2} - \kappa n(n-1)\right)C^g_n(t) - ig_2\sqrt{n+1}C^e_{n+1}(t). \tag{C18}$$

When the initial states meet $C^e_{n+1}(0) = 1$ and $C^g_n(0) = 0$, we then get the time-evolution equation of the system state as

$$|\phi(t)\rangle = \left[\left(\cos\frac{\Omega^{\rm AJC}_n t}{2} - \frac{i\xi + 2\kappa n}{\Omega^{\rm AJC}_n}\sin\frac{\Omega^{\rm AJC}_n t}{2}\right)|n+1, e\rangle - i\frac{2g_2\sqrt{n+1}}{\Omega^{\rm AJC}_n}\sin\frac{\Omega^{\rm AJC}_n t}{2}|g, n\rangle\right]e^{-i(n+1/2)\omega t - \kappa n^2 t}. \tag{C19}$$

We then obtain the time-dependent population on state $|n, g\rangle$,

$$P^{\rm AJC}_{|n,g\rangle} = \frac{4g_2^2(n+1)}{\left(\Omega^{\rm AJC}_n\right)^2}\sin^2\left(\frac{\Omega^{\rm AJC}_n t}{2}\right). \tag{C20}$$

APPENDIX D: FURTHER DISCUSSION OF THE PARITY-TIME SYMMETRY

The energy spectrum of the JCM with two-photon dissipation is characterized by $\mathcal{PT}$ symmetry and the presence of exceptional points. Based on the above calculation, the eigenvalues of this system at resonance are

$$E^{\rm JC}_{n,\pm} = \left(n + \tfrac{1}{2}\right)\omega - i\kappa n^2 \pm \sqrt{g_1^2(n+1) - \kappa^2 n^2}, \tag{D1}$$

where $-i\kappa n^2$ is interpreted as a frequency shift. For $g^2(n+1) > \kappa^2 n^2$, the radical term has a real value, whereas for $g^2(n+1) < \kappa^2 n^2$, the value becomes the imaginary form

$$E^{\rm JC}_{n,\pm} = \left(n + \tfrac{1}{2}\right)\omega - i\kappa n^2 \pm i\sqrt{\kappa^2 n^2 - g_1^2(n+1)}. \tag{D2}$$

According to the energy spectrum of the JCM with two-photon dissipation when $n = 1$, the energy level splitting is closed at $g_1/\omega = \kappa/\sqrt{2}$ and the imaginary part of the energy after this position is a constant $-i\kappa$, which means the entire system has one dissipation channel at the same rate. In this case, it can be regarded as a passive $\mathcal{PT}$ system. The imaginary part of the energy level is zero after the crossing point by shifting the imaginary part of the energy level. The region of all-real eigenvalues corresponds to the $\mathcal{PT}$-symmetric phase of the system, as shown in the darker part of Fig. 8. Generally, the system reaches an exceptional point when $\delta = 0$, and the position is

$$g_1^{\rm EP} = \sqrt{\frac{\kappa^2 n^2}{n+1}}. \tag{D3}$$

which varies with the photon number n.

APPENDIX E: IMPACT OF ONE-PHOTON DISSIPATION

The two-photon loss mechanism has been theoretically explored and experimentally realized [28–34]. Therefore, this dissipation mechanism has its practical importance. If small single-photon dissipation is present, a direct consequence is that the Z_2 symmetry of the dissipative system will be broken and the dynamics in different parity chains will be mixed.

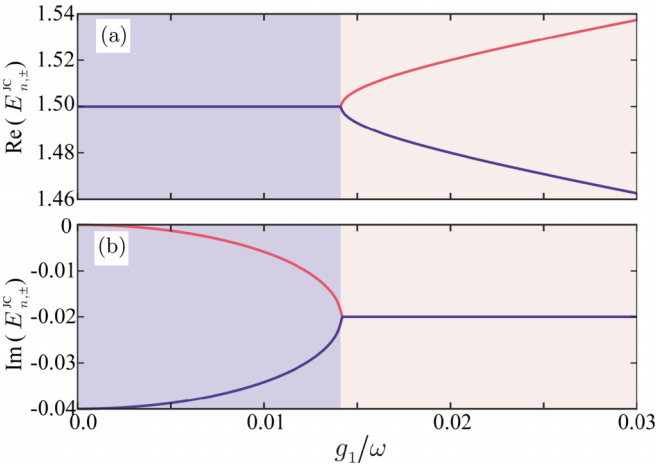

FIG. 8. Energy spectrum of the JCM with two-photon dissipation when $\Delta = \omega$ and $n = 1$: (a) real and (b) imaginary parts of the splitting energy levels $E^{\rm JC}_{1,+}$ (red line) and $E^{\rm JC}_{1,-}$ (blue line). It can be observed that there is an energy overlap at $g_1/\omega = \sqrt{2} \times 10^{-2}$.

To confirm this prediction, we have conducted additional simulations that include a small single-photon dissipation rate. In Table I we briefly summarize our numerical results with different one-photon decay rates γ and two-photon decay rates κ, followed by more detailed discussion.

When the single-photon decay rate $\gamma/\omega = 0.001$ is much smaller than the two-photon dissipation $\kappa/\omega = 0.02$, the dynamics of the system is influenced to a minimal degree by the single-photon process. In this case, the two-photon dissipation process dominates the system's relaxation; thus the transient states in short periods are still parity sensitive. Since the effect of single-photon dissipation continues to mix the evolution processes in the two parity chains, the final steady states are independent of the parity of initial states.

With simultaneous considerable single-photon and two-photon dissipation processes, e.g., $\gamma/\omega = 0.01$ and $\kappa/\omega = 0.02$, the parity sensitivities and the avoided crossings due to the strong mixing of the energy states vanish gradually. When only the single-photon dissipation rate exists, with $\gamma/\omega = 0.01$ and $\kappa/\omega = 0$, the system becomes stable after some period of oscillation. The dynamics of the mean photon number and the qubit population in both transient and steady states do not have any distinct properties owing to the parity of initial states.

TABLE I. Parity dependence of the system dynamics with different dissipation parameters.

Parameter regime	Parity dependence in transient states	Parity dependence in steady states
$\gamma \ll \kappa$	yes	no
$\gamma \approx \kappa$	no	no
$\gamma \gg \kappa$	no	no

APPENDIX F: SUPERPOSITION STATES AS INITIAL STATES

Our theoretical model has Z_2 symmetry corresponding to the conservation of parity. This ensures that any initial state with definite parity only evolves within its parity subspace. If an initial state is a superposition of two states from different parity subspaces, the components will still evolve independently in their definite subspaces. In this case, however, the overall superposed state does not have definite parity. For this scenario, we have set the initial state as $(|2, g\rangle + |3, g\rangle)/\sqrt{2}$ and the calculated dynamics confirmed the predictions.

The superposition within a parity subspace deserves further discussion. We consider the superposition of two bare states in the same parity chain as the initial state. This scenario has two distinct cases, depending on whether these two bare states are nearest neighbors or next-nearest neighbors.

For the nearest-neighbor case, the dynamics of the system with initial states $(|2, g\rangle + |3, e\rangle)/\sqrt{2}$ (even parity) and $(|3, g\rangle + |4, e\rangle)/\sqrt{2}$ (odd parity) is calculated. The evolution processes and strengths of the two nearest-neighboring bare states are different, leading to the absence of any distinctive features in the dynamics corresponding to this superposition of states. However, the overall dynamical behavior remains parity sensitive.

For the next-nearest-neighbor case, we calculated the dynamics of $(|2, g\rangle + |4, g\rangle)/\sqrt{2}$ (even parity) and $(|3, g\rangle + |5, g\rangle)/\sqrt{2}$ (odd parity) as the initial states, respectively. We found that the dynamical behaviors are consistent with those of the bare states $|2, g\rangle$ and $|3, g\rangle$, respectively. This is because the bare states at higher energy levels quickly radiate to the lower levels by the two-photon dissipation processes through $|4, g\rangle \Rightarrow |2, g\rangle$ and $|5, g\rangle \Rightarrow |3, g\rangle$ and then undergo the same dissipative dynamics as the lower states.

The more complicated initial states, such as coherent states and cat states, can be understood as a combination of the superposition discussed above, and thus the resulting dynamics can be predicted.

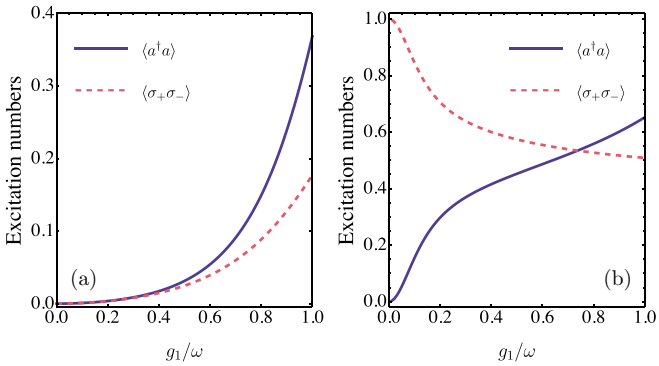

FIG. 9. Final steady states of mean photon numbers and qubit populations in (a) even- and (b) odd-parity subspaces.

APPENDIX G: STEADY STATES VERSUS QUASISTEADY STATES

To further clarify the difference between the final steady and quasisteady states shown in Figs. 3(h) and 4(h), we calculate the mean photon number and qubit population with respect to the coupling strength g_1 in the final steady state through the Lindblad master equation.

The steady state in even-parity subspace, displayed in Fig. 9(a), is similar to that of the quasisteady state in Fig. 3(h), but the peaks that exist in the quasisteady state are absent. In the odd-parity subspace, Fig. 4(h) and the corresponding analysis show that the oscillations persist and it takes a long time to arrive at the steady state. Therefore, the steady state in Fig. 9(b) is rather different from the quasisteady state in Fig. 4(h), especially in the regimes with relatively small coupling strengths.

[1] I. I. Rabi, On the process of space quantization, Phys. Rev. **49**, 324 (1936).

[2] D. Braak, Integrability of the Rabi model, Phys. Rev. Lett. **107**, 100401 (2011).

[3] Q. Xie, H. Zhong, M. T. Batchelor, and C. Lee, The quantum Rabi model: Solution and dynamics, J. Phys. A: Math. Theor. **50**, 113001 (2017).

[4] D. Braak, Q.-H. Chen, M. T. Batchelor, and E. Solano, Semi-classical and quantum Rabi models: In celebration of 80 years, J. Phys. A: Math. Theor. **49**, 300301 (2016).

[5] S. Ashhab and F. Nori, Qubit-oscillator systems in the ultrastrong-coupling regime and their potential for preparing nonclassical states, Phys. Rev. A **81**, 042311 (2010).

[6] H. Zhong, Q. Xie, M. T. Batchelor, and C. Lee, Analytical eigenstates for the quantum Rabi model, J. Phys. A: Math. Theor. **46**, 415302 (2013).

[7] H. Zhong, Q. Xie, X. Guan, M. T. Batchelor, K. Gao, and C. Lee, Analytical energy spectrum for hybrid mechanical systems, J. Phys. A: Math. Theor. **47**, 045301 (2014).

[8] V. Vedral, *Modern Foundations of Quantum Optics* (Imperial College Press, London, 2006).

[9] H. G. Reik, H. Nusser, and L. A. A. Ribeiro, Exact solution of non-adiabatic model Hamiltonians in solid state physics and optics, J. Phys. A: Math. Gen. **15**, 3491 (1982).

[10] M. Wagner, *Unitary Transformations in Solid State Physics* (North-Holland, Amsterdam, 1986).

[11] F. Yoshihara, T. Fuse, S. Ashhab, K. Kakuyanagi, S. Saito, and K. Semba, Superconducting qubit–oscillator circuit beyond the ultrastrong-coupling regime, Nat. Phys. **13**, 44 (2017).

[12] A. F. Kockum, A. Miranowicz, S. D. Liberato, S. Savasta, and F. Nori, Ultrastrong coupling between light and matter, Nat. Rev. Phys. **1**, 19 (2019).

[13] Q.-H. Chen, L. Li, T. Liu, and K.-L. Wang, The spectrum in qubit-oscillator systems in the ultrastrong coupling regime, Chin. Phys. Lett. **29**, 014208 (2012).

[14] Z.-M. Li and M. T. Batchelor, Generalized adiabatic approximation to the quantum Rabi model, Phys. Rev. A **104**, 033712 (2021).

[15] Z.-M. Li, D. Ferri, and M. T. Batchelor, Nonorthogonal-qubit-state expansion for the asymmetric quantum Rabi model, Phys. Rev. A **103**, 013711 (2021).
[16] Z.-M. Li and M. T. Batchelor, Algebraic equations for the exceptional eigenspectrum of the generalized Rabi model, J. Phys. A: Math. Theor. **48**, 454005 (2015).
[17] M. T. Batchelor and H.-Q. Zhou, Integrability versus exact solvability in the quantum Rabi and Dicke models, Phys. Rev. A **91**, 053808 (2015).
[18] Z.-M. Li and M. T. Batchelor, Hidden symmetry and tunneling dynamics in asymmetric quantum Rabi models, Phys. Rev. A **103**, 023719 (2021).
[19] X. Lu, Z.-M. Li, V. V. Mangazeev, and M. T. Batchelor, Hidden symmetry in the biased Dicke model, J. Phys. A: Math. Theor. **54**, 325202 (2021).
[20] V. V. Mangazeev, M. T. Batchelor, and V. V. Bazhanov, The hidden symmetry of the asymmetric quantum Rabi model, J. Phys. A: Math. Theor. **54**, 12LT01 (2021).
[21] X. Lu, H. Li, J.-K. Shi, L.-B. Fan, V. Mangazeev, Z.-M. Li, and M. T. Batchelor, $\mathcal{PT}$-symmetric quantum Rabi model, Phys. Rev. A **108**, 053712 (2023).
[22] S. Ashhab, Superradiance transition in a system with a single qubit and a single oscillator, Phys. Rev. A **87**, 013826 (2013).
[23] M.-J. Hwang, R. Puebla, and M. B. Plenio, Quantum phase transition and universal dynamics in the Rabi model, Phys. Rev. Lett. **115**, 180404 (2015).
[24] M. Liu, S. Chesi, Z.-J. Ying, X. Chen, H.-G. Luo, and H.-Q. Lin, Universal scaling and critical exponents of the anisotropic quantum Rabi model, Phys. Rev. Lett. **119**, 220601 (2017).
[25] X.-Y. Chen, Y.-Y. Zhang, L. Fu, and H. Zheng, Generalized coherent-squeezed-state expansion for the super-radiant phase transition, Phys. Rev. A **101**, 033827 (2020).
[26] M. Wolinsky and H. J. Carmichael, Quantum noise in the parametric oscillator: From squeezed states to coherent-state superpositions, Phys. Rev. Lett. **60**, 1836 (1988).
[27] M. Malekakhlagh and A. W. Rodriguez, Quantum Rabi model with two-photon relaxation, Phys. Rev. Lett. **122**, 043601 (2019).
[28] M. Mirrahimi, Z. Leghtas, V. V. Albert, S. Touzard, R. J. Schoelkopf, L. Jiang, and M. H. Devoret, Dynamically protected cat-qubits: A new paradigm for universal quantum computation, New J. Phys. **16**, 045014 (2014).
[29] Z. Leghtas, G. Kirchmair, B. Vlastakis, M. H. Devoret, R. J. Schoelkopf, and M. Mirrahimi, Deterministic protocol for mapping a qubit to coherent state superpositions in a cavity, Phys. Rev. A **87**, 042315 (2013).
[30] Z. Leghtas, G. Kirchmair, B. Vlastakis, R. J. Schoelkopf, M. H. Devoret, and M. Mirrahimi, Hardware-efficient autonomous quantum memory protection, Phys. Rev. Lett. **111**, 120501 (2013).
[31] D. I. Schuster, A. A. Houck, J. A. Schreier, A. Wallraff, J. M. Gambetta, A. Blais, L. Frunzio, J. Majer, B. Johnson, M. H. Devoret, S. M. Girvin, and R. J. Schoelkopf, Resolving photon number states in a superconducting circuit, Nature (London) **445**, 515 (2007).
[32] Z. Leghtas, S. Touzard, I. M. Pop, A. Kou, B. Vlastakis, A. Petrenko, K. M. Sliwa, A. Narla, S. Shankar, M. J. Hatridge, M. Reagor, L. Frunzio, R. J. Schoelkopf, M. Mirrahimi, and M. H. Devoret, Confining the state of light to a quantum manifold by engineered two-photon loss, Science **347**, 853 (2015).
[33] N. Ofek, A. Petrenko, R. Heeres, P. Reinhold, Z. Leghtas, B. Vlastakis, Y. Liu, L. Frunzio, S. M. Girvin, L. Jiang, M. Mirrahimi, M. H. Devoret, and R. J. Schoelkopf, Extending the lifetime of a quantum bit with error correction in superconducting circuits, Nature (London) **536**, 441 (2016).
[34] C. Wang, Y. Y. Gao, P. Reinhold, R. W. Heeres, N. Ofek, K. Chou, C. Axline, M. Reagor, J. Blumoff, K. M. Sliwa, L. Frunzio, S. M. Girvin, L. Jiang, M. Mirrahimi, M. H. Devoret, and R. J. Schoelkopf, A Schrödinger cat living in two boxes, Science **352**, 1087 (2016).
[35] Q.-T. Xie, S. Cui, J.-P. Cao, L. Amico, and H. Fan, Anisotropic Rabi model, Phys. Rev. X **4**, 021046 (2014).
[36] M. Tomka, O. El Araby, M. Pletyukhov, and V. Gritsev, Exceptional and regular spectra of a generalized Rabi model, Phys. Rev. A **90**, 063839 (2014).
[37] G. Zhang and H. Zhu, Analytical solution for the anisotropic Rabi model: Effects of counter-rotating terms, Sci. Rep. **5**, 8756 (2015).
[38] C. Joshi, J. Larson, and T. P. Spiller, Quantum state engineering in hybrid open quantum systems, Phys. Rev. A **93**, 043818 (2016).
[39] G. Wang, R. Xiao, H. Z. Shen, C. Sun, and K. Xue, Simulating anisotropic quantum Rabi model via frequency modulation, Sci. Rep. **9**, 4569 (2019).
[40] C. Sánchez Muñoz, A. Frisk Kockum, A. Miranowicz, and F. Nori, Simulating ultrastrong-coupling processes breaking parity conservation in Jaynes-Cummings systems, Phys. Rev. A **102**, 033716 (2020).
[41] Z.-J. Ying, Symmetry-breaking patterns, tricriticalities, and quadruple points in the quantum Rabi model with bias and nonlinear interaction, Phys. Rev. A **103**, 063701 (2021).
[42] Z.-J. Ying, From quantum Rabi model to Jaynes–Cummings model: Symmetry-breaking quantum phase transitions, symmetry-protected topological transitions and multicriticality, Adv. Quantum Technol. **5**, 2100088 (2022).
[43] S. Wang, S. Chen, J. Jing, J. Wang, and H. Fan, Quantum collapse and exponential growth of out-of-time-ordered correlator in anisotropic quantum Rabi model, arXiv:2305.17495.
[44] X. Zhu, J.-H. Lü, W. Ning, F. Wu, L.-T. Shen, Z.-B. Yang, and S.-B. Zheng, Criticality-enhanced quantum sensing in the anisotropic quantum Rabi model, Sci. China: Phys. Mech. Astron. **66**, 250313 (2023).
[45] H.-G. Xu, V. Montenegro, G. Xianlong, J. Jin, and G. D. d. M. Neto, Persisting quantum effects in the anisotropic Rabi model at thermal equilibrium, Phys. Rev. Res. **6**, 013001 (2024).
[46] Y.-Y. Zhang and X.-Y. Chen, Analytical solutions by squeezing to the anisotropic Rabi model in the nonperturbative deep-strong-coupling regime, Phys. Rev. A **96**, 063821 (2017).
[47] Y. Wang, Y. Zhang, C. Li, J. Wei, B. He, H. Xu, J. Xia, X. Luo, J. Li, J. Dong, W. He, Z. Yan, W. Yang, F. Ma, G. Chai, P. Yan, C. Wan, X. Han, and G. Yu, Ultrastrong to nearly deep-strong magnon-magnon coupling with a high degree of freedom in synthetic antiferromagnets, Nat. Commun. **15**, 2077 (2024).
[48] J. Casanova, G. Romero, I. Lizuain, J. J. García-Ripoll, and E. Solano, Deep strong coupling regime of the Jaynes-Cummings model, Phys. Rev. Lett. **105**, 263603 (2010).
[49] K. Wilma, C.-C. Shu, U. Scherf, and R. Hildner, Visualizing hidden ultrafast processes in individual molecules by

single-pulse coherent control, J. Am. Chem. Soc. **140**, 15329 (2018).

[50] K. Wilma, C.-C. Shu, U. Scherf, and R. Hildner, Two-photon induced ultrafast coherence decay of highly excited states in single molecules, New J. Phys. **21**, 045001 (2019).

[51] D. Manzano, A short introduction to the Lindblad master equation, AIP Adv. **10**, 025106 (2020).

[52] E. T. Jaynes and F. W. Cummings, Comparison of quantum and semiclassical radiation theories with application to the beam maser, Proc. IEEE **51**, 89 (1963).

[53] L.-B. Fan, Y.-H. Zhou, F. Zou, H. Guo, J.-F. Huang, and J.-Q. Liao, Quantum thermalization and vanishing thermal entanglement in the open Jaynes-Cummings model, Ann. Phys. (Berlin) **532**, 2000134 (2020).

[54] L.-B. Fan, C.-C. Shu, D. Dong, J. He, N. E. Henriksen, and F. Nori, Quantum coherent control of a single molecular-polariton rotation, Phys. Rev. Lett. **130**, 043604 (2023).

[55] L.-B. Fan and C.-C. Shu, Pulse-area theorem for precision control of the rotational motions of a single molecule in a cavity, J. Phys. A: Math. Theor. **56**, 365302 (2023).